ISIJ International, Vol. 61 (2021), No. 1, pp. 401–407
https://doi.org/10.2355/isijinternational.ISIJINT-2020-256

Estimation of Lankford Coefficients of Austenitic and Ferritic Stainless Steels using Mean Grain Orientations from Micro-texture Measurements

Suresh KODUKULA,[1,2)]* Timo MANNINEN[1)] and David PORTER[2)]

1) Outokumpu Process R&D, Tornio, 95490 Finland.
2) Materials and Mechanical Engineering, Centre for Advanced Steels Research, University of Oulu, 90014 Finland.

(*Received on April 29, 2020; accepted on September 11, 2020; J-STAGE Advance published date: November 4, 2020*)

A new method to calculate the plastic anisotropy r-values of austenitic and ferritic stainless steels has been developed. The mean orientation of individual grains is obtained from SEM-EBSD data and r-values for individual grains are calculated by weighting all slip systems according to their Schmid factors. Calculated and measured r-values are in good agreement for austenitic stainless steels. However, in ferritic stainless steels, which are highly anisotropic, good agreement requires the introduction of a Schmid factor threshold below which slip systems are inactive. The present method can be used to estimate local differences in r-values in ferritic stainless steels showing the local variations in texture responsible for ridging.

KEY WORDS: austenitic stainless steels; ferritic stainless steels; planar anisotropy; Schmid factor; r-value; Lankford coefficient; mean grain orientation; orientation density function.

1. Introduction

The plastic strain ratio, also referred to as the r-value or the Lankford coefficient, is a basic formability index of importance in deep drawing. This is generally measured in tensile tests after 10–15% strain and is the ratio of the true strains in the width and thickness directions. A high r-value implies high resistance to thinning and a high limit drawing ratio, *i.e.* improved formability in deep drawing. The r-value is unity in a material with a random texture, but in cubic metals with non-random textures, it may range from 0.5 to 2.5. The presence of texture also introduces variations in r-value with the orientation of the tensile direction in the sheet.[1,2)]

Hosford and Backofen[3)] proposed a method for calculating the mechanical properties affected by texture. Their approach was an extension of Taylor's analysis for cubic metals and was based on finding the combination of slip systems that minimizes the amount of slip to a accomplish a given strain. Veith and Whiteley[4)] presumed that slip occurs on one or more equally favorably oriented slip systems having the highest resolved shear stress, *i.e.* the largest Schmid factor (SF). Chao[5)] used a single slip system with highest SF to calculate the normal anisotropy in various materials. An attempt was made by Chao to assess whether the texture combinations and distributions present in ferritic stainless steels can explain the ridging phenomenon. The use of only one active slip system, however, results in r-value equal to zero or infinity for certain tensile directions. Fukuda *et al.*[6)] chose the five slip systems with the highest SFs. Lee *et al.*[7,8)] extended the approach by weighting each slip system with its SF.

Various properties of textured polycrystalline materials can be estimated from crystal orientation distribution functions (ODFs) obtained by X-ray diffraction (XRD) or scanning electron microscopy (SEM) combined with electron backscattered diffraction (EBSD).[2)] In early studies, planar anisotropy calculations were often limited to three or four ideal orientations whose intensities were evaluated using either ODF or pole figures from the XRD measurements.[3–5,7–11)] The planar anisotropy calculations calculated with these formulations are generally in good agreement for FCC systems such as copper and aluminum alloys. When only using the intensities of the main texture components for BCC ferritic stainless steel (FSS) and carbon steels, however, large discrepancies are found between measured and calculated r-values. Such is the case when calculations are based on active slip systems or Taylor analyses.[7,11–15)] One of the key reasons for the large discrepancy is the strong texture gradient that exists in cold-rolled ferritic stainless steels through the thickness.[14,16–18)] To account for the texture gradient in the BCC metals, XRD-measurements are usu-

* Corresponding author: E-mail: suresh.kodukula@outokumpu.com

© 2021 The Iron and Steel Institute of Japan. This is an open access article under the terms of the Creative Commons Attribution-NonCommercial-NoDerivs license (https://creativecommons.org/licenses/by-nc-nd/4.0/).

ally conducted on various planes through the thickness, but it remains unclear whether enough measurements have been conducted to fully capture the details of the texture gradient. The influence of the texture gradient has been studied by Hamada *et al.*[19] by stacking sheets of FSS and measuring the overall texture using XRD on a through-thickness cross-section perpendicular to the transverse direction (TD) and comparing this with textures obtained at various depths through the thickness on sections perpendicular to the thickness, *i.e.* the sheet normal direction (ND). They concluded that for a sample with a strong texture gradient, it is impossible to precisely calculate the planar anisotropy (r-value) from the texture of a particular ND-section.

Taylor full constraint (FC) and relaxed constraint (RC) models have been proposed for the prediction of deformation textures and the resulting anisotropy in cold-rolled and annealed sheet metals.[11–14,19,20] According to Jonas *et al.*,[12] for BCC alloys, the best quantitative agreement between measured and predicted anisotropy is achieved when the critical resolved shear stress (CRSS) ratio of the {112} <111> and {110} <111> slip systems is 0.95. In the case of FSS, Hamada *et al.*[17] investigated the effect of {112} <111>/{110} <111> CRSS ratio in the range 0.9–1.1 using the relaxed constraint model RC1323 and claimed that the ratio 1.1 was most suitable for predicting the planar anisotropy. Du *et al.*[21] conducted micro-pillar tests on single crystal ferrite from interstitial free (IF) steel and concluded that both {110} and {112} slip systems contribute to the deformation at room temperature the {123} system is not activated. They also found that the CRSS for the {110} and {112} slip systems are very close. These experimental findings on ferritic steel emphasize that having the parameters controlling the activation of different slip systems play a critical role in obtaining the good prediction of macroscopic material properties. Although many models have been proposed for predicting the normal anisotropy of in sheet metals, in most cases, they only consider three or four ideal texture components, and also fail to properly address the inherent through-thickness texture gradient in FSS.

EBSD measurements on through-thickness cross-sections give the orientations of individual grains, but this kind of detailed textural information has so far never been used for predicting r-values. ODF's obtained from X-ray diffraction pole figures are often considered as a reference for the accuracy of EBSD results. According to Hutchinson *et al.*[22] better texture could be evaluated using EBSD measurements, as orientations can be determined with an accuracy of 1° provided the probed area is large enough. Of course, it is important to measure a sufficient number of grains to obtain a representative ODF. Engler *et al.*[23] and Baudin *et al.*[24] proposed that 1 500 single grain orientations are needed to calculate the ODF from EBSD data. By comparing ODF's obtained with an ever increasing number of grains, Bozzolo *et al.*[25] showed that an ODF evaluated using 5 000 grains is accurate and acceptable. In the present study, EBSD measurements are conducted on commercial cold-rolled and annealed austenitic and ferritic stainless steel sheets, *i.e.* both FCC and BCC materials. The texture gradient in the BCC material is carefully accounted for by conducting EBSD measurements on three through-thickness sections. The actual orientations of all grains are used to calculate the planar anisotropies of these materials on the basis of a new simple modelling approach. It will be shown that the modelled r-values agree well with those measured using tensile testing on samples oriented at various angles to the rolling direction (RD). The use of EBSD data to calculate r-values can also be valuable in the study of the ridging phenomenon in ferritic stainless steels.

2. Materials and Methods

The chemical composition of the cold-rolled and annealed, 1-mm thick, commercial austenitic EN 1.4404 and ferritic EN 1.4622 stainless steels used in this study are given in **Table 1**. Tensile tests were conducted using a Zwick Z250/SW5A tensile testing machine according to the standard ISO EN 6892-1 using three specimens per orientation at 0°, 15°, 30°, 45°, 60°, 75° and 90° to the rolling direction. **Tables 2** and **3** give the average values obtained from the tests. The r-values were measured after a tensile elongation of 15% for the ferritic grade and 20% for the austenitic grade.

Electron back scattered diffraction (EBSD) measurements were carried out in a scanning electron microscope (SEM) (1450VP) to measure the micro-texture of the samples. The

Table 1. Chemical composition of austenitic grade EN 1.4404 and ferritic grade EN 1.4622 (wt.%).

Grade	C	Si	Cr	Ni	Mn	Mo	N	Ti	Nb
EN 1.4404	0.022	0.5	16.7	10.1	0.9	2.0	0.045	–	–
EN 1.4622	0.015	0.45	21	–	0.3	2.0	0.015	0.15	0.25

Table 2. Mechanical properties of austenitic stainless steel grade EN 1.4404. Averages of three specimens per direction. ± values are the uncertainty in the measurement for the confidence level of 95% observed over many tests.

Angle to Rolling Direction (°)	$R_{P0.2}$ (N/mm^2)	$R_{P1.0}$ (N/mm^2)	R_m (N/mm^2)	A_{80} (%)	r-value (−)
0	262 ± 5	290 ± 6	576 ± 3	48.0 ± 0.5	0.61 ± 0.03
15	262 ± 5	290 ± 6	575 ± 3	49.0 ± 0.5	0.66 ± 0.03
30	263 ± 5	293 ± 6	575 ± 3	50.0 ± 0.5	0.80 ± 0.03
45	266 ± 5	295 ± 6	576 ± 3	52.0 ± 0.5	1.01 ± 0.03
60	272 ± 5	300 ± 6	582 ± 3	52.6 ± 0.5	1.22 ± 0.03
75	276 ± 5	303 ± 6	586 ± 3	54.0 ± 0.5	1.32 ± 0.03
90	276 ± 5	302 ± 6	586 ± 3	55.3 ± 0.5	1.29 ± 0.03

© 2021 ISIJ

Table 3. Mechanical properties of ferritic stainless steel grade EN 1.4622. Averages of three specimens per direction. ± values are the uncertainty in the measurement for the confidence level of 95% observed over many tests.

Angle to Rolling Direction (°)	$R_{P0.2}$ (N/mm^2)	$R_{P1.0}$ (N/mm^2)	R_m (N/mm^2)	A_{80} (%)	r-value (−)
0	343 ± 6	356 ± 7	495 ± 2	32.1 ± 0.3	1.60 ± 0.03
15	352 ± 6	365 ± 7	501 ± 2	32.2 ± 0.3	1.43 ± 0.03
30	365 ± 6	376 ± 7	509 ± 2	30.0 ± 0.3	1.27 ± 0.03
45	372 ± 6	381 ± 7	515 ± 2	30.3 ± 0.3	1.28 ± 0.03
60	375 ± 6	384 ± 7	514 ± 2	30.6 ± 0.3	1.56 ± 0.03
75	368 ± 6	376 ± 7	503 ± 2	31.8 ± 0.3	1.98 ± 0.03
90	364 ± 6	372 ± 7	499 ± 2	32.9 ± 0.3	2.12 ± 0.03

SEM measurements were conducted with a step size of 1.5 μm at an accelerating voltage of 20 kV. Texture data was obtained using Oxford HKL acquisition and analysis software. For the austenitic EN 1.4404 specimen, measurements were conducted on a TD-ND cross-section. Due to the presence of a texture gradient in the ferritic grade, the SEM-EBSD measurements were carried out on three cross-sections, *i.e.* 1) RD-ND, 2) 45° to RD (45-ND) and 3) TD-ND. Orientation distribution functions (ODFs) were calculated using the M-TEX toolbox.[26–28)]

3. Numerical

The r-value is given by the ratio of width to thickness strain (ϵ_w/ϵ_T) in a tensile test.[29,30)] Vieth and Whiteley[4)] derived the following relation for calculating the r-value in the case of single slip

$$r = \frac{\varepsilon_w}{\epsilon_t} = \frac{\left|(w \cdot d)(w \cdot n)\right|}{\left|(t \cdot d)(t \cdot n)\right|} \quad \text{..... (1)}$$

where w and t are unit normal vectors in the width and thickness directions, and d and n are unit vectors in the slip direction and the direction normal to the slip plane. To calculate the plastic strain ratio from Eq. (1), the operating slip system must be selected, which is taken as that with the highest SF. Lee *et al.*[5)] proposed that r-values can also be calculated by considering all the slip systems weighted according to their SFs. Hence Eq. (1) can be expanded to include all slip systems weighted in proportion to their SFs. Considering one grain orientation at a time, like in visco-plastic calculations,[31)] for the ith orientation strained at an angle θ to the RD we have

$$r_{\theta,i} = \frac{\varepsilon_w}{\varepsilon_t} = \frac{\sum_{j=1}^{ss}\left|(w_\theta \cdot d_j)(w_\theta \cdot n_j)m_{\theta,j}\right|}{\sum_{j=1}^{ss}\left|(t_\theta \cdot d_j)(t_\theta \cdot n_j)m_{\theta,j}\right|} \quad \text{..... (2)}$$

$$m_{\theta,j} = \left|(l_\theta \cdot d_j)(l_\theta \cdot n_j)\right| \quad \text{..... (3)}$$

where j is the slip system, $m_{\theta,j}$ is the SF of the jth slip system, and l_θ is a unit vector along the tensile direction. For the material as a whole, the overall r-value is calculated by summing the contributions of the various orientations weighted according their intensity in the ODF, *i.e.*

$$r_\theta = \frac{\sum_{i=1}^{N} r_{\theta,i}\, f(g_i)}{\sum_{i=1}^{N} f(g_i)} \quad \text{..... (4)}$$

where r_θ is the overall plastic strain ratio of the specimen for the direction θ, $r_{\theta,i}$ is the plastic strain ratio contribution of the ith orientation. g_i is the mean orientation of ith grain and $f(g_i)$ is the texture intensity of the orientation which is obtained from the ODF using the M-TEX toolbox[26–28)] as units of multiples of uniform distribution (MUD).

For the FCC austenitic stainless steels, r-values are calculated by including all 12 {111} <110> slip systems. For the BCC FSS 24 slip systems are considered, *i.e.* {110} <111> and {112} <111>, and in line with the findings of Du *et al.*,[21)] it is assumed that $CRSS_{(110)} = CRSS_{(112)}$.

4. Results

4.1. r-value of Austenitic Stainless Steel

Figure 1 shows an EBSD inverse pole figure (IPF) measured over the full 1 mm thickness and a length of 2 mm on a TD-ND cross-section of the austenitic grade. The image comprises a total of 9 940 grains with an average grain diameter of 21.24 μm. **Figure 2** shows the corresponding ODF at φ_2 = 45°. The mean orientations of individual grains are obtained from the EBSD data and are used to calculate the r-values. In the calculations, all 12 {111} <110> slip systems are considered, and their strain contributions are weighted in proportion to the corresponding SFs. The contribution of all the grains in a given orientation (g) to the overall r-value is and the normal anisotropy of the material in the direction of strain is evaluated after normalizing their texture intensities for all the grains as shown in Eq. (4). The r-values calculated this way are in good agreement with those measured using tensile test specimens as shown in **Fig. 3**.

4.2. r-value of Ferritic Stainless Steel

An EBSD-IPF map for a full-thickness TD-ND cross-section 3.68 mm in length along the transverse direction of the ferritic stainless-steel specimen is shown in **Fig. 4**. It comprised 17 962 grains with an average grain diameter of 19.87 μm. The ODF is shown at φ_2 = 45° in **Fig. 5**. The ODF intensity is between 0 and 5 and illustrates that the specimen has a strong texture with weak cube orientations and a very strong gamma (γ) fiber which enhances the deep drawing properties. In addition to the above, EBSD measurements were also made on two other full-thickness cross-sections: 1) an RD-ND section 7.32 mm in length along rolling direction comprising 33 795 grains, and 2) a

© 2021 ISIJ

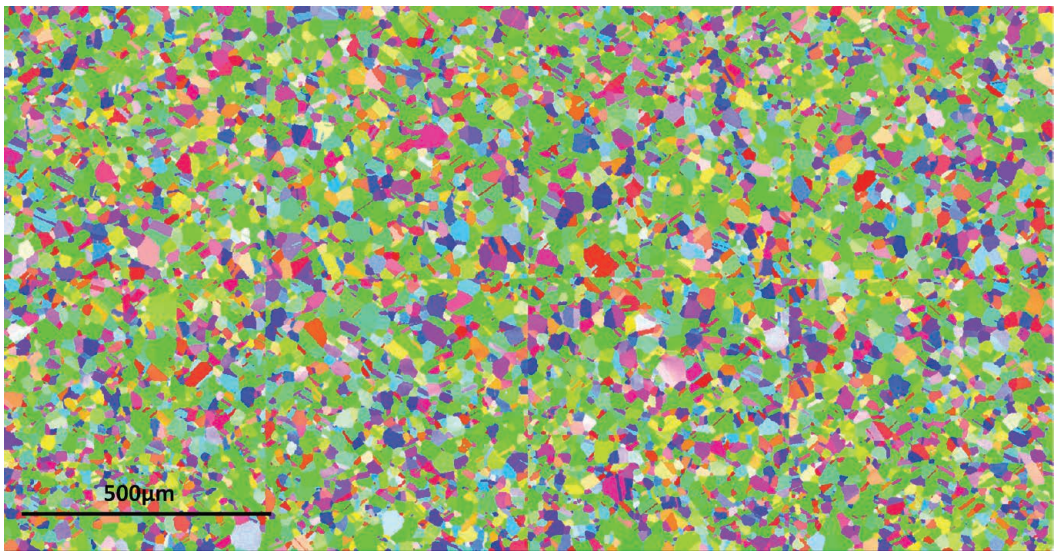

Fig. 1. Stitched EBSD-IPF image of a TD-ND cross-section through the austenitic stainless steel specimen. Color code refers to the crystallographic orientation of the ND direction. (Online version in color.)

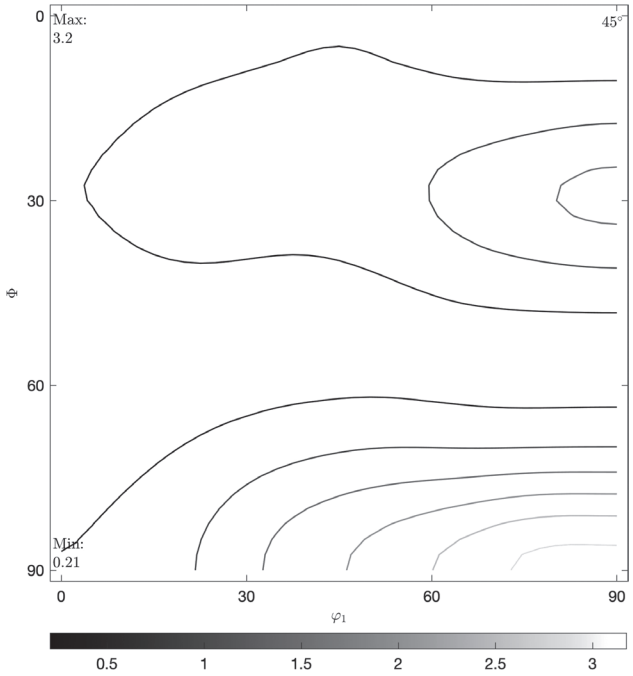

Fig. 2. ODF of the austenitic stainless steel sample at $\varphi_2 = 45°$. The contour lines are at an interval of 0.5 units.

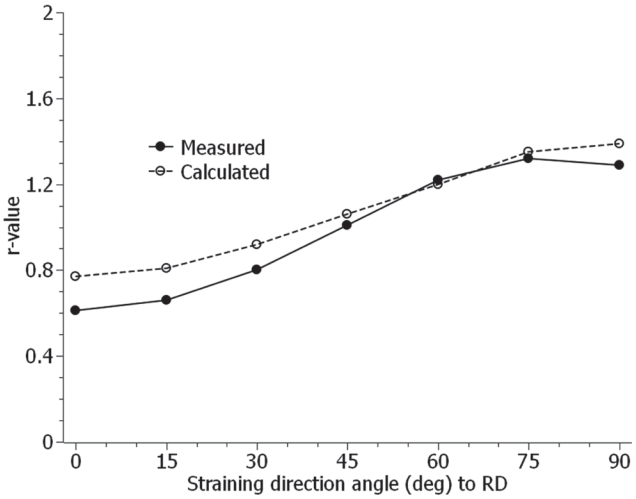

Fig. 3. Planar anisotropy of r-values measured vs calculated from the EBSD-texture for the austenitic stainless steel specimen.

7.33 mm long section at 45° to RD (denoted 45-ND) comprising 35 189 grains.

Figure 6 shows the calculated r-values considering all 24 slip systems of the type {110} <111> and {112} <111> using the mean grain orientations measured on the RD-ND, TD-ND and 45-ND cross-sections. The r-values obtained from tensile testing are also included for comparison. All three cross-sections give essentially identical results as the orientations observed are also similar. Although, the grain size is not considered in the present r-value calculations, the grain size distributions of all the cross-sections were compared to find any variations in the grain size. **Figure 7** shows the grain size distributions. The average grain sizes are 19.87, 20.88 and 20.65 μm respectively in RD-ND, TDND and 45-ND cross sections.

5. Discussion

5.1. Schmid Factor Threshold and Active Slip Systems

Unlike the FCC structure of the austenitic stainless steel, the BCC structure of the FSS has no single family of high-density slip planes. Generally, the slip planes in BCC are {110} and {112} and the slip direction is <111> giving 24 possible slip systems compared to the 12 {111} <110> slip systems in FCC. The measured and calculated r-values are in very good agreement for the austenitic stainless steel when considering all 12 slip systems to be active and weighting their contribution according to their SFs; however, this was not the case for the FSS. Similar observations have been made earlier[7,8,13,19] with good agreement between calculated and measured r-values for FCC materials such as aluminum and brass, but poor agreement for BCC carbon steel and ferritic stainless steel.

Yazawa *et al.*[32] reported that FSS and mild steel show good correlations between {111} texture intensity and average r-values, but that for the same level of {111} intensity,

© 2021 ISIJ

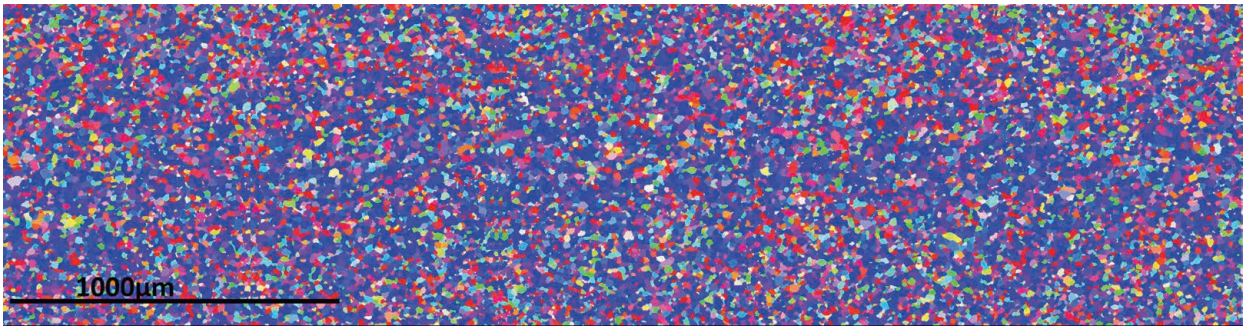

Fig. 4. Stitched EBSD-IPF image of a TD-ND cross-section through the ferritic stainless steel specimen. Color code refers to the crystallographic orientation of the ND direction. (Online version in color.)

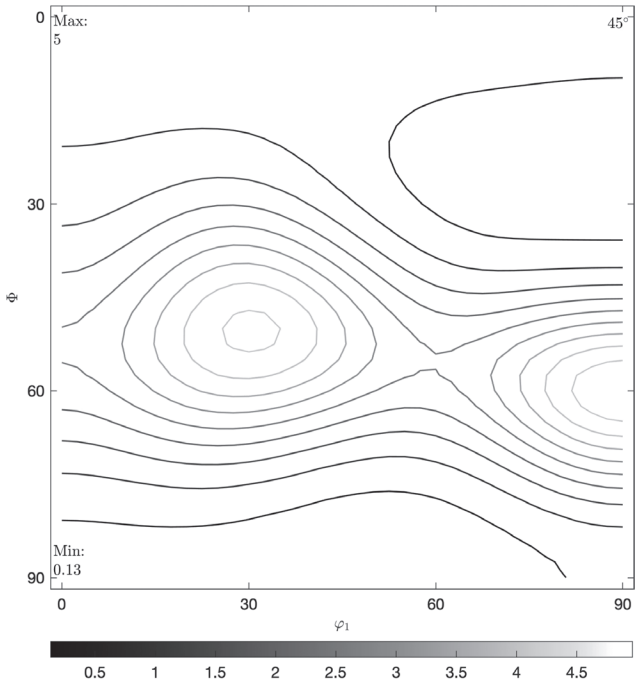

Fig. 5. ODF of the ferritic stainless steel at $\varphi_2 = 45°$ and the contour lines are at an interval of 0.5 units.

FSS had higher r-values than mild steel. The addition of chromium to iron promotes the formation of twinning, which has been shown to suppress slip on {112} planes.[28] Hamada[19] showed that r-values calculated assuming slip is limited to {110} <111> are higher than calculated by considering both {110} <111> and {112} <111> slip systems to be active. This demonstrates that limiting the operative slip systems increases planar anisotropy.

The operating slip systems can be reduced by introducing a minimum SF, below which the slip system is inactive. Doing this for all the tensile directions from 0° to 90° shows that the best results are found to be when the threshold SF is in the range 0.22–0.29. The calculated values with the SF threshold at 0.29 are in good match when the tensile direction is 0 and 90, whereas the calculated and measured r-values match well when the SF threshold is 0.22 along 45° to RD. The higher r-value regions are in good agreement when using the higher SF threshold while the lower SF threshold is better for the lower r-value regions. The measured and calculated r-values with SF thresholds of 0.22 and 0.29 are shown in **Fig. 8**.

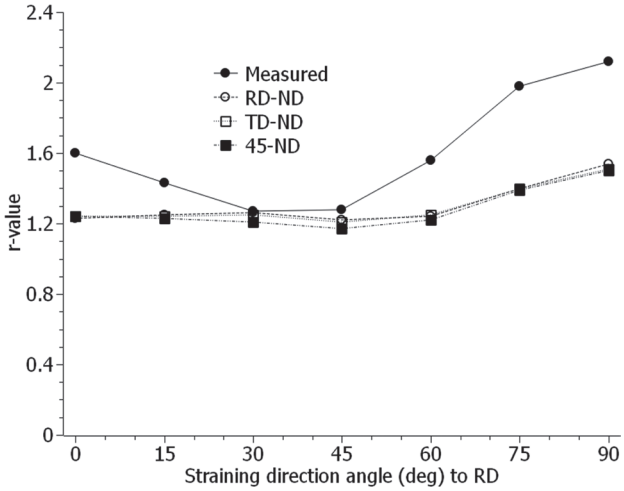

Fig. 6. Measured vs calculated planar anisotropy of r-values using grain orientations found on the RD-ND, TD-ND and 45-ND cross-sections of the ferritic steel.

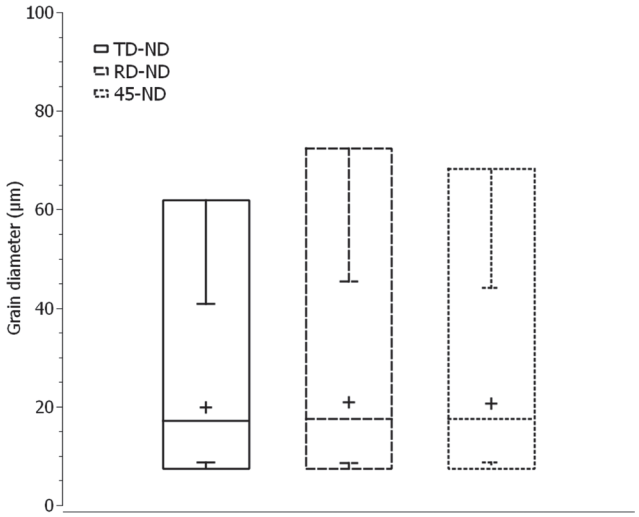

Fig. 7. Boxplot of the grain diameters of the ferritic stainless steel on the cross-sections TD-ND, RD-ND and 45-ND. The boxes show the 1st, 50th and 99th percentiles and the whiskers indicate 5th and 75th percentiles. The plus (+) sign represents the mean grain diameter which are 19.87, 20.88 and 20.65 μm respectively.

5.2. The Effect of Tensile Direction on Schmid Factor Threshold

Crystallographic texture plays crucial role in anisotropy as witnessed by the differences in the textures and degrees

© 2021 ISIJ

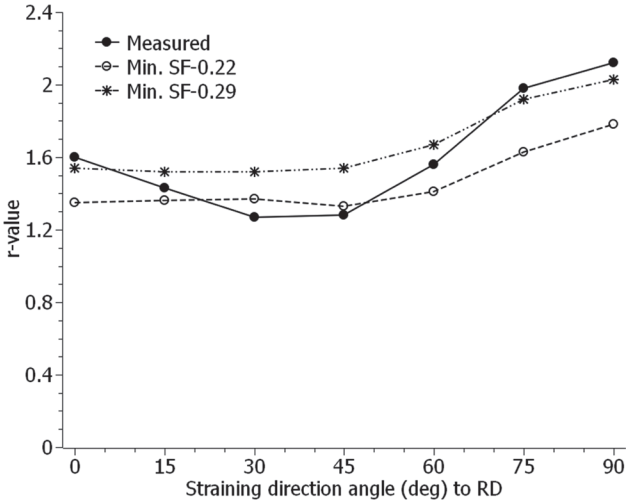

Fig. 8. Calculated planar anisotropy of r-values for the TD-ND plane using the slip systems with SF ≥ 0.29 (*) and SF ≥ 0.22 (o). Measured r-values shown for comparison (filled circles).

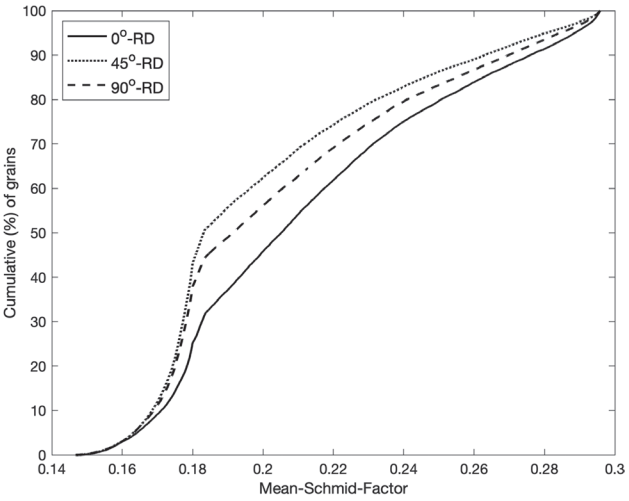

Fig. 9. Grain mean SF distributions for straining in 0, 45 and 90 degrees to RD for the TD-ND section of ferritic stainless steel specimen (BCC).

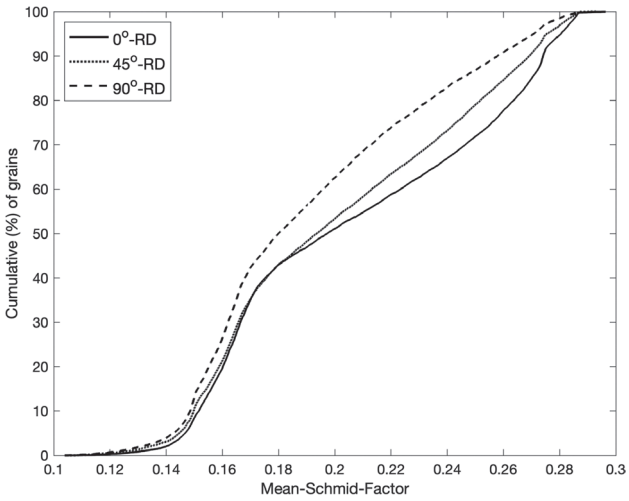

Fig. 10. Grain mean SF distributions for straining in 0, 45 and 90 degrees to RD for the TD-ND section of austenitic stainless steel specimen (FCC).

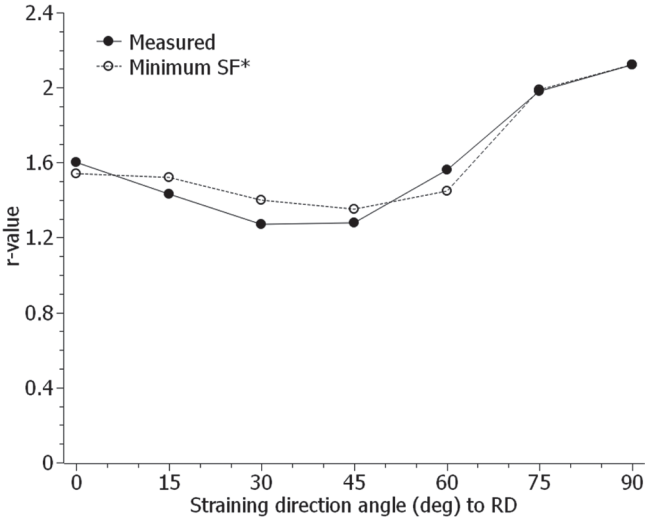

Fig. 11. r-values calculated using a cut-off SF of 0.29 for 0°, 15°, 75° and 90° to RD, and 0.22 for 30°, 45° and 60° to RD.

of planar anisotropy in the present FCC and BCC materials. The variation of the threshold SF with tensile direction needs to be rationalized. Due to the texture in the FSS, a change in the tensile direction causes a change in the levels of the SFs on the 24 slip systems in each grain. This is reflected in the SF averaged over all 24 slip systems in the grains. **Figure 9** shows cumulative frequency distributions of the mean SF of the 16 000 grains on the TD-ND section for straining along 0°, 45° and 90° to the RD. Similarly, **Fig. 10** shows the mean SF of the 9 940 grains of the austenitic stainless steel. The distributions of the mean SF in the FCC austenitic stainless and BCC FSS obviously differ, and in the case of the FCC material introducing a minimum operative SF threshold would have the same influence in all straining directions and the r-values would increase along all directions. On the other hand, for the FSS, Fig. 9 shows that when the tensile axis is at 45° to the RD the SFs are generally lower than they are for the RD or TD directions. The highest SFs are obtained with the tensile axis at 0°. The cumulative mean SF distributions agree with the tensile test results in Table 3: the flow stress at a plastic strain of 1% ($R_{p1.0}$) for example is highest when the tensile axis is at 45° to the RD and lowest when it is at 0°. This is to be expected as plastic flow requires the product of SF and applied stress to exceed the CRSS. Returning to the cumulative SF distributions in Fig. 9 and the calculated r-values in Fig. 8, the cut-off values for the SFs follow the same trend as median SFs, for example. Therefore, a high cut-off value for the 0° and 90° tensile directions and a low value for the 45° tensile direction may limit the number of active slip systems in the grains to the same extent irrespective of the tensile direction. A good agreement between the measured and calculated r-values is obtained by selecting the cut-off values as shown in **Fig. 11**.

6. Summary and Conclusions

In this study, plastic strain ratios (r-values) for several straining directions relative to the rolling direction have been calculated from the overall texture determined from EBSD measurements on full-thickness cross-sections. The

© 2021 ISIJ

individual mean grain orientations were used to calculate the r-value using all the slip systems weighted according to their SFs. r-values calculated for the austenitic stainless steel considering all 12 slip systems are in good agreement with values obtained from tensile tests. However, for the FSS there is no quantitative agreement between the calculated and measured r-values when using the same approach and all 24 {110}–{112} slip systems ignoring any possible dependence of the CRSS on the slip plane. Good agreement is obtained by introducing threshold SFs, *i.e.* minimum values of the SF for a slip system to be active, the values of which depend on the straining direction relative to the RD. The threshold SF is highest for those directions with the highest r-values and lowest for directions with the lowest r-values. This method can be applied to materials with high through-thickness or transverse texture gradients as the orientations of individual grains are used in the plastic anisotropy calculations. Such an approach can find application in the study of ridging phenomenon in ferritic stainless steels for example.

REFERENCES

1) P. Paufler: *Cryst. Res. Technol.*, **29** (1994), 532.
2) B. Hutchinson: *Mater. Sci. Technol.*, **31** (2015), 1393. https://doi.org/10.1179/1743284715Y.0000000118
3) W. Hosford and W. Backofen: Proc. 9th Sagamore Conf., (New York), Syracrause University Press, New York, (1964), 259.
4) R. W. Vieth and R. L. Whiteley: IDDRG Colloquium, (London), London Institute of Sheet Metal Engineering, London, (1964), 20.
5) H. Chao: *Trans. Am. Soc. Met.*, **60** (1967), 37.
6) M. Fukuda: *Trans. Iron Steel Inst. Jpn.*, **8** (1968), 68.
7) D. N. Lee and K. H. Oh: *J. Mater. Sci.*, **20** (1985), 3111.
8) D. N. Lee: *J. Korean Inst. Met.*, **20** (1982), 586.
9) R. N. Wright: *Metall. Trans.*, **3** (1972), 83.
10) D. Lee: *Mater. Sci. Forum*, **449**–**452** (2004), 1. https://doi.org/10.4028/www.scientific.net/MSF.449-452.1
11) H. Shin, J. An, S. Park and D. N. Lee: *Acta Mater.*, **51** (2003), 4693. https://doi.org/10.1016/S1359-6454(03)00187-3
12) D. Daniel and J. Jonas: *Metall. Trans. A*, **21** (1990), 331.
13) P. Welch and H. Bunge: *Mater. Sci. Technol.*, **2** (1986), 354.
14) J. Hamada, K. Agata and H. Inoue: *Mater. Trans.*, **50** (2009), 752. https://doi.org/10.2320/matertrans.MRA2008399
15) J. Hamada, Y. Matsumoto, F. Fudanoki and S. Maeda: *ISIJ Int.*, **43** (2003), 1989. https://doi.org/10.2355/isijinternational.43.1989
16) D. Raabe and K. Lücke: *Scr. Metall. Mater.*, **26** (1992), 1221.
17) D. Raabe and K. Lücke: *Mater. Sci. Technol.*, **9** (1993), 302.
18) J. Mola, D. Chae and B. C. De Cooman: *Solid State Phenom.*, **160** (2010), 153.
19) J. Hamada, N. Ono and H. Inoue: *ISIJ Int.*, **51** (2011), 1740.
20) G. Lefebvre, S. Shahandeh, C. Sinclair, M. Militzer, J. D. Mithieux and J. Laigo: *Mater. Sci. Forum*, **715**–**716** (2012), 866.
21) C. Du, F. Maresca, M. G. D. Geers and J. P. M. Hoefnagels: *Acta Mater.*, **146** (2018), 314. https://doi.org/10.1016/j.actamat.2017.12.054
22) W. B. Hutchinson, E. Lindh and P. Bate: Proc. 12th Int. Conf. on Textures of Materials (ICOTOM 12), (Montreal), NRC Press, Ottawa, (1999), 34.
23) O. Engler, G. Gottstein, J. Pospiech and J. Jura: *Mater. Sci. Forum*, **157**–**162** (1994), 259.
24) T. Baudin, J. Jura, R. Penelle and J. Pospiech: *J. Appl. Crystallogr.*, **28** (1995), 582.
25) N. Bozzolo, F. Gerspach, G. Sawina and F. Wagner: *J. Microsc.*, **227** (2007), 275.
26) R. Hielscher and H. Schaeben: *J. Appl. Crystallogr.*, **41** (2008), 1024.
27) R. Hielscher, H. Schaeben and H. Siemes: *Math. Geosci.*, **42** (2010), 359.
28) F. Bachmann, R. Hielscher and H. Schaeben: *Ultramicroscopy*, **111** (2011), 1720.
29) U. Dehlinger: *Angew. Chem.*, **48** (1935), 518.
30) H. Biloni and W. Boettinger: Physical Metallurgy, Vol. 1, eds. by R. W. Cahn and P. Haasen, North Holland, Amsterdam, (1996), 669.
31) R. Lebensohn and C. Tomé: *Acta Metall. Mater.*, **41** (1993), 2611. https://doi.org/10.1016/0956-7151(93)90130-K
32) Y. Yazawa, Y. Ozaki, Y. Kato and O. Furukimi: *JSAE Rev.*, **24** (2003), 483.

© 2021 ISIJ